Structural and Functional Characterization of Second-Coordination Sphere Mutants of Soybean Lipoxygenase-1[†]

Diana R. Tomchick,[‡] Phuc Phan,[§] Marcin Cymborowski,[‡] Wladek Minor,*[,‡] and Theodore R. Holman*[,§]

Department of Molecular Physiology and Biological Physics, University of Virginia, Charlottesville, Virginia 22908, and Departments of Chemistry and Biochemistry, University of California, Santa Cruz, California 95064

Received December 20, 2000; Revised Manuscript Received April 26, 2001

ABSTRACT: Lipoxygenases are an important class of non-heme iron enzymes that catalyze the hydroperoxidation of unsaturated fatty acids. The details of the enzymatic mechanism of lipoxygenases are still not well understood. This study utilizes a combination of kinetic and structural probes to relate the lipoxygenase mechanism of action with structural modifications of the iron's second coordination sphere. The second coordination sphere consists of Gln_{495} and Gln_{697}, which form a hydrogen bond network between the substrate cavity and the first coordination sphere (Asn_{694}). In this investigation, we compared the kinetic and structural properties of four mutants (Q495E, Q495A, Q697N, and Q697E) with those of wild-type soybean lipoxygenase-1 and determined that changes in the second coordination sphere affected the enzymatic activity by hydrogen bond rearrangement and substrate positioning through interaction with Gln_{495}. The nature of the C−H bond cleavage event remained unchanged, which demonstrates that the mutations have not affected the mechanism of hydrogen atom tunneling. The unusual and dramatic inverse solvent isotope effect (SIE) observed for the Q697E mutant indicated that an Fe(III)-OH^- is the active site base. A new transition state model for hydrogen atom abstraction is proposed.

Lipoxygenases are widely distributed throughout the plant and animal kingdoms and serve a variety of vital roles in biology. In plants, they are involved in immunity, growth regulation, and germination (*1*, *2*). In mammals, lipoxygenases produce leukotrienes and lipoxins, which constitute an important family of signaling molecules that affect a number of biological processes, such as asthma, atherosclerosis, and cancer (*3*−*8*). Lipoxygenases are a class of non-heme iron enzymes which catalyze the incorporation of dioxygen into 1,4-*cis*,*cis*-pentadiene-containing fatty acids (e.g., linoleic and arachidonic acids) to form hydroperoxide products (*9*). The essential iron atom is in the inactive, ferrous oxidation state, as isolated, and is activated by 1 equiv of hydroperoxide product [(9*Z*,11*E*)-13-hydroperoxy-9,11-octadecadienoic acid (13-HPOD)][1] which oxidizes the iron to the ferric state. The most widely accepted reaction mechanism for the hydroperoxidation is radical-based, where the fatty acid is oxidized by the ferric iron to form a fatty acid radical and a ferrous iron (*10*, *11*). This ferrous−substrate radical intermediate is then attacked regio- and stereospecifically by dioxygen, to form only the S-configured product. Klinman and co-workers have demonstrated that below 30 °C, k_{cat}/K_m is limited by diffusion, the solvent isotope, and hydrogen abstraction (*12*).

The X-ray crystal structures of the ferrous form of wild-type soybean lipoxygenase-1 (SLO) have been determined by two groups (*13*−*15*). Both have identified two structural domains, an N-terminal β-sandwich and a C-terminal α-helical region, the latter of which contains the active site iron. Four common active site iron ligands were reported by both groups, His_{499}, His_{504}, His_{690}, and the terminal carboxylate of Ile_{839}, each of these being conserved in all the sequenced lipoxygenases (one exception is rat leukocyte 5-lipoxygenase which has a valine at the C-terminus). Boyington et al. described the active site as four-coordinate with two adjacent unoccupied ligand positions, whereas Minor et al. identified six ligands: the four ligands mentioned above, an additional water ligand, and a distant Asn_{694} (3.06 Å). The bound water points directly toward the mouth of the proposed substrate-binding channel. EXAFS measurements show a water bound to the iron that changes to a hydroxide upon oxidation, which is proposed to function as the active site base; however, there is no kinetic evidence to support this (*16*).

Residue Gln_{495} lines the putative substrate cavity wall and begins an extensive hydrogen bond network that stretches toward the metal and may provide a structural link between substrate binding and iron coordination (*15*). Gln_{495} hydrogen bonds to Gln_{697}, which in turn hydrogen bonds to Asn_{694}, a weak, first-coordination sphere ligand (Figure 2a). A similar hydrogen bond network is observed in the rabbit 15-lipoxygenase (15-RLO) structure, where Glu_{357} is equivalent

[†] This work was supported by NIH Grant GM56062-01 (T.R.H.) and partly by NIH Grant GM53163 and DOE/SBC grants (W.M.).

* To whom the correspondence should be addressed. T.R.H.: phone, (831) 459-5884; fax, (831) 459-2935; e-mail, tholman@chemistry.ucsc.edu. W.M.: phone, (804) 243-6865; fax, (804) 982-1616; e-mail, wladek@iwonka.med.virginia.edu.

[‡] University of Virginia.

[§] University of California.

[1] Abbreviations: SLO, wild-type soybean lipoxygenase-1; Q495E, Gln495Glu SLO; Q495A, Gln495Ala SLO; Q495N, Gln495Asn SLO; Q697N, Gln697Asn SLO; Q697E, Gln697Glu SLO; LA-H31, linoleic acid; LA-D31, perdeuterated linoleic acid; 13-HPOD, 13-hydroperoxy-9(*Z*),11(*E*)-octadecadienoic acid; ICP-MS, inductively coupled plasma mass spectroscopy; MCD, magnetic circular dichroism; EXAFS, extended X-ray absorption fine structure.

10.1021/bi002893d CCC: $20.00
Published on Web 06/02/2001

to Gln_{495} and Gln_{548} is equivalent to Gln_{697} (*17*). This hydrogen bond network in 15-RLO plays an important role in defining the inhibitor binding site as seen by the close interaction between the bound inhibitor and Glu_{357}. MCD data showed that substrate binding changed the coordination environment of the ferrous iron from a mixture of five- and six-coordinate to a purely six-coordinate iron, which may be due to the hydrogen bond network (*19*). In the absence of an actual substrate complex,[2] we have decided to investigate this hypothesis further in an indirect fashion by mutating residues in the hydrogen bond network (Q495E, Q495A, Q697E, and Q697A) in an effort to determine whether these residues affect catalysis by changing the iron environment and/or the structure of the substrate cavity.

MATERIALS AND METHODS

Materials. Restriction endonucleases and polynucleotide kinase were obtained from New England BioLabs (Beverly, MA). 13-HPOD was HPLC purified from the reaction mixture of SLO and linoleic acid (LA-H31), as previously described (*20*). LA-H31 was purchased from Aldrich Chemical Co., and perdeuterated linoleic acid (LA-D31) was purified from a mixture of perdeuterated algal fatty acids from Cambridge Isotope Laboratories, as previously described (*21*). All other reagents were reagent grade or better and were used without further purification.

Plasmids, Expression, and Purification of Proteins. Plasmids for the mutagenesis (pL-1) and overproduction (pT-7/L-1) of SLO were provided by B. Axelrod. Site-directed mutagenesis was carried out by the Kunkel method with pL-1, as previously described (*20*). All genes were sequenced in the area near the mutation to verify the presence of only the expected mutations. The protein plasmid was then transformed into *Escherichia coli* BL21(DE3), expressed, and purified as described previously (*20*). All mutants were expressed as soluble proteins. The expression of Q495N was also attempted; however, a soluble protein could not be obtained.

Enzyme activities were determined by monitoring the absorption of the product formed during the enzymatic reaction at 234 nm ($\epsilon_{234} = 25\,000\ M^{-1}\ cm^{-1}$). The iron content of all lipoxygenase enzymes was determined via a Finnegan ICP-MS apparatus, using standardized iron solutions (*20*). All kinetic measurements were standardized to iron content.

Kinetic Isotope Effect and Steady State Kinetic Measurements. Determination of the competitive kinetic isotope effect (KIE) for k_{cat}/K_m was achieved with the established HPLC method, as previously described by Holman and co-workers (*21*, *22*). Steady state kinetics and steady state KIE values were determined by following the formation of product at 234 nm ($\epsilon_{234} = 25\,000\ M^{-1}\ cm^{-1}$) with a Hewlett-Packard 8453 UV−vis spectrophotometer. All reaction mixtures were 2 mL in volume [0.1 M borate (pH 9.2)] and were constantly stirred with a rotating magnetic bar. Enzymatic rates were measured over a range of substrate concentrations (between 1 and 64 μM LA-H31), and each substrate solution was measured for accurate [LA-H31] determination by quantitatively converting the substrate to product. Rate reactions were initiated by the addition of enzyme to final enzyme concentrations of ≈3 nM or until the activity was ≈0.01 abs/s at 64 mM LA-H31 for slower mutants. All kinetic parameters were determined by nonlinear regression using Kaleidagraph software (Abelbeck), as described previously (*21*).

Viscosity Dependence. Buffer and substrate solutions of 0 and 30 wt % glucose, in 0.1 M CHES buffer at pH 9.2 and 22 °C, were prepared corresponding to relative viscosities (η_{rel}) of 1 and 3, respectively ($\eta_{rel} = \eta/\eta^\circ$, η° is the viscosity of H_2O at 22 °C, from the *CRC Handbook of Chemistry*). Sucrose and ethylene glycol were not used as viscogenic agents due to inhibition of SLO, and borate was not used because it reacts with glucose to lower its buffering capacity (*12*).

Solvent Isotope Effect Determination. Kinetic measurements were performed with either LA-H31 or LA-D31 in 50 mM borate in H_2O or D_2O, 16 mM NaCl (a total ionic concentration of 40 mM), pL 9.2 (pH meter reading of 8.8 for D_2O), at temperatures of 22 and 5 °C. SIE measurements were taken in three different experiments, and the values were averaged.

EPR Spectroscopy. EPR measurements were performed on a Bruker ESP 320 spectrometer fitted with a dielectric resonator and companion helium cryostat, as described previously (*20*). The EPR spectra were measured with a microwave power of 31 μW (4.3 K) and determined to be well below the level of power saturation.

UV−Vis CD Spectroscopy. CD spectra were obtained at 10 °C using an Aviv 60DS spectrophotometer. CD spectra are baseline corrected by subtracting the reduced enzyme spectrum from the oxidized enzyme spectrum. Titrations were performed by the addition of 1 equiv of 13-HPOD (evaporated) to 0.6 mL of lipoxygenase (20 mg/mL) (*20*).

Crystallization and Data Collection. Crystals of soybean L-1 lipoxygenase mutants were grown and cryocooled as described previously (*15*, *23*) with a few modifications. Sitting drops (5 μL of 4 mg/mL protein with 5 μL of well solution) were equilibrated in a plastic Cryschem tray versus 0.75 mL of 9% PEG 3350 and 0.2 M sodium acetate (pH 5.5) for 2 days. The drops were microseeded with serial dilutions of a fresh seed stock prepared by crushing a large crystal in 20 μL of well solution. Single crystals appeared the next day, and generally reached maximum size after 3 weeks.

Diffraction data from all mutants were collected at the Structural Biology Center 19-ID beamline of the Advanced Photon Source, with the use of APS1 or SBC-2 CCD detectors (*24*). All data were collected at 100 K. The multipass data collection mode has been used as described previously (*15*). All mutant crystals belonged to space group *P2*(1) and were isomorphous with the wild-type soybean L-1 crystals. All data were processed and scaled in the HKL2000 program suite (*25*). Intensities were converted to structure factor amplitudes and placed on an approximate absolute scale by the program TRUNCATE from the CCP4 package (*26*, *27*). Data collection and processing statistics are summarized in Table 1.

[2] While there are three-dimensional structures of small molecule inhibitors bound to lipoxygenases (*17*, *18*), to date there are no structures of an enzyme−substrate complex. The limited solubility of substrates and substrate mimics, especially at the low pH and relatively high ionic strength of the crystallization media, has complicated this effort.

Table 1: Data Collection Statistics

	Q495E	Q495A	Q697N	Q697E
wavelength	0.97918	0.97918	0.97918	1.03321
data range (Å)	99.0−1.85	99.0−1.62	99.0−1.62	20.0−1.60
cell dimensions				
a (Å)	93.2	94.2	94.3	94.4
b (Å)	92.6	92.8	92.8	92.8
c (Å)	49.2	49.4	49.4	49.4
β (deg)	90.37	90.46	90.41	90.09
no. of observations	274097	592213	490154	481538
no. of unique observations	70275	104379	104489	101615
completeness (%)	98.9	96.6	96.8	91.2
R_{sym} (%)	5.5	4.5	4.3	6.4

Crystallographic Refinement. Refinement of the wild-type and mutant structures was carried out in the program package CNS 1.0 with a random 5% subset of all data set aside for an R_{free} calculation. Fe−ligand bond lengths and geometries were not explicitly restrained (*28*). Initial model coordinates for each mutant were obtained through modifying the wild-type coordinates by replacing the mutated residue with an alanine. Rigid-body refinement of the model coordinates versus data with d_{min} ranging from 20.0 to 3.0 Å was conducted, followed by a cycle of standard positional and group isotropic thermal factor refinement versus data with d_{min} ranging from 20.0 Å to the high-resolution limit for each structure. Inspection of electron-density maps in the program O allowed a model for the mutated side chain to be built in each mutant structure (*29*). Subsequent cycles of standard positional and individual isotropic thermal factor refinement coupled with cycles of model rebuilding, modeling of alternate conformations, and addition of solvent sites were carried out against all data with d_{min} ranging from 20.0 Å to the appropriate high-resolution limit for each structure. During the initial cycles of refinement of the Q697E and Q697N mutant structures, an examination of difference Fourier maps revealed that the Fe site was not fully occupied. In the final cycles of refinement, the occupancy of the Fe was fixed to 0.63 for Q697E and 0.7 for Q697N, which resulted in an isotropic temperature factor (31.6 and 24.22 Å^2, respectively) for the Fe that matched the average for the Fe ligands (31.3 and 22.14 Å^2, respectively). Complete refinement statistics for all structures can be found in Table 2.

RESULTS

Mutagenesis, Expression, and Purification. Mutant SLO enzymes yielded approximately 5 mg/L and were greater than 90% pure, as judged by SDS−PAGE (stained with Coomassie brilliant blue, data not shown) (*20*).

Kinetic Analysis of Mutant Soybean Lipoxygenase-1. As isolated, ICP-MS indicated that the mutant enzymes contained, on average, greater than 0.7 mol of iron per mole of enzyme. The calculated k_{cat}, K_m, and k_{cat}/K_m values at 22 and 5 °C were corrected for iron content (Table 3). The k_{cat} data at 22 °C for Q495E (329 ± 15 s^{-1}) indicated that it was the most similar in rate to SLO (287 ± 5 s^{-1}); however, its k_{cat}/K_m value (14 ± 2 s^{-1} μM^{-1}) was slightly lower than that of SLO (19 ± 1 s^{-1} μM^{-1}). Q495A and Q697N displayed a decrease in k_{cat} (68 ± 2 and 98 ± 5 s^{-1}, respectively), which was the primary reason for their lowered k_{cat}/K_m rates (5.7 ± 0.5 and 6.5 ± 1 s^{-1} μM^{-1}, respectively). Q697E displayed the lowest kinetic parameters of all the second-coordination sphere mutants, with decreases in both k_{cat} (45 ± 2 s^{-1}) and k_{cat}/K_m (2.1 ± 0.2 s^{-1} μM^{-1}).

The kinetics at 5 °C revealed a decrease in k_{cat}/K_m for all the enzymes that were studied (Table 3). The k_{cat} values for all the mutant enzymes decreased in a manner consistent with the k_{cat}/K_m data. The k_{cat} of Q495E was not determined because its K_m(app) had increased to the point where

Table 2: Refinement Statistics

	wild type	Q495E	Q495A	Q697N	Q697E
total no. of non-hydrogen atoms	7403	7218	7444	7341	7210
no. of water sites	897	703	843	768	587
data range (Å)	20.0−1.40	20.0−1.85	20.0−1.62	20.0−1.62	20.0−1.60
no. of reflections	151073	70251	104247	104391	101592
R (%)	19.8	18.0	18.8	18.2	19.6
R_{free} (%)	21.2	21.4	22.3	21.3	22.2
mean *B* value (Å^2)					
main chain	21.4	28.9	22.4	21.7	31.9
side chain	23.3	31.2	24.5	24.4	34.5
rms deviations from target values					
bonds (Å)	0.0098	0.0098	0.0098	0.0097	0.0093
angles (deg)	1.43	1.51	1.48	1.52	1.48
Luzzati error	0.18	0.20	0.19	0.18	0.20
missing residues	1−5, 19−30, 117−120	1−5, 21−30, 118−121	1−5, 20−31, 117−121	1−6, 21−31, 116−121	1−5, 22−30, 118−121
no. of alternate conformations	17	6	13	10	9
PDB accession code	1f8n	1fgq	1fgo	1fgt	1fgr

Table 3: Kinetic Parameters for SLO and Second-Sphere Mutants at 22 and 5 °C[a]

	k_{cat}(22 °C)	K_m(22 °C)	k_{cat}/K_m(22 °C)	k_{cat}(5 °C)	K_m(5 °C)	k_{cat}/K_m(5 °C)	Fe (%)
SLO	287 (5)	15 (1)	19 (1)	60 (4)	17 (3)	3.5 (0.7)	75 (4)
Q495E	329 (15)	23 (3)	14 (2)	n/d[b]	n/d[b]	1.4 (0.1)	75 (4)
Q495A	68 (2)	12 (1)	5.7 (0.5)	38 (1)	13 (1)	2.9 (0.2)	95 (5)
Q697N	98 (5)	15 (2)	6.5 (1)	41 (3)	29 (4)	1.4 (0.2)	70 (4)
Q697E	45 (2)	21 (2)	2.1 (0.2)	29 (1)	23 (2)	1.3 (0.1)	85 (5)

[a] In 100 mM borate (pH 9.2). k_{cat} is per second. K_m is in micromolar. k_{cat}/K_m is in per second per micromolar. [b] Not determined (see the Results).

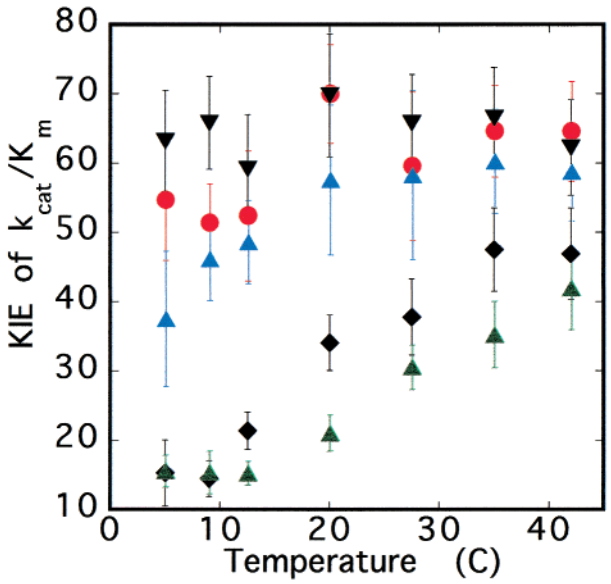

FIGURE 1: Results of variable-temperature k_{cat}/K_m KIE experiments with SLO (black diamonds), Q697N (blue triangles), Q697E (black inverted triangles), Q495E (green triangles), and Q495A (red circles). The reactions were run to 5% completion with a 5 μM LA-H31/LA-D31 mixture in 100 mM borate buffer (pH 9.2).

substrate saturation could not be achieved due to limited substrate solubility. The k_{cat}/K_m was measured from the linear region of the initial velocity, where [LA] $\ll K_m$.

Competitive Kinetic Isotope Effect. Previously, we showed that SLO displays temperature-dependent competitive KIE results for k_{cat}/K_m at a low substrate concentration (5 μM) (*22*). This temperature dependence is due to multiple rate-limiting steps in the mechanism: substrate diffusion, hydrogen bond rearrangement (or water exclusion), and C−H bond cleavage (*12*). Q495E exhibited a rise in the k_{cat}/K_m KIE, similar to that of SLO (Figure 1). Q697N exhibited a temperature-independent KIE above 20 °C and a slight decrease in KIE below 20 °C, indicating a greater dependence of Q697N on C−H bond cleavage than of both SLO and Q495E (Figure 1). Q495A and Q697E displayed a very small temperature dependence of their k_{cat}/K_m KIE which indicates almost complete dependence of the rate-determining step on C−H bond cleavage (Figure 1). These data were tempered by the fact that there was a high degree of error in KIE at low temperatures for both Q495A and Q697E, which could mask a greater temperature dependence of their KIEs.

Viscosity Measurements. SLO is a fast enzyme that is 50% diffusion limited (k_{cat}/K_m = 19 s^{-1} μM^{-1} at 22 °C), which indicates that if the viscosity of the buffer solution is increased, the k_{cat}/K_m rate will decrease (i.e., SIE > 1) (*12*, *21*). Viscosity dependence experiments were performed on the SLO-1 mutants [$(k_{cat}/K_m°)/(k_{cat}/K_m)$, where $\eta/\eta°$ = 1 and 3] which demonstrate that some of the mutants are no longer rate-limited by diffusion (Table 4). At 22 °C, the k_{cat}/K_m was insensitive to increasing viscosity for Q495A, Q697N, and Q697E [$(k_{cat}/K_m°)/(k_{cat}/K_m) \approx 1$], which indicated that diffusion of substrate was not rate-limiting. However, the k_{cat}/K_m values for SLO [$(k_{cat}/K_m°)/(k_{cat}/K_m) = 1.8 \pm 0.1$] and Q495E [$(k_{cat}/K_m°)/(k_{cat}/K_m) = 1.5 \pm 0.1$] were reduced by increasing viscosity, showing that they were partially rate-limited by diffusion at 22 °C (Table 4). At 5 °C, SLO, Q495E, and Q697N were sensitive to viscosity, which indicated they are still partially limited by diffusion, while Q495A and Q697E were not.

Table 4: Viscosity Dependence at 5 and 22 °C (0 and 30% glucose)[a]

	$(k_{cat}/K_m°)/(k_{cat}/K_m)$(22 °C)	$(k_{cat}/K_m°)/(k_{cat}/K_m)$(5 °C)
SLO	1.8 (0.1)	1.5 (0.1)
Q495E	1.5 (0.1)	1.5 (0.1)
Q495A	1.1 (0.1)	1.1 (0.1)
Q697N	1.1 (0.1)	1.5 (0.2)
Q697E	0.92 (0.1)	1.1 (0.1)

[a] In 100 mM Ches (pH 9.2).

Table 5: Solvent Isotope Effect at 22 and 5 °C (H_2O/D_2O) with LA-H31[a]

	k_{cat}(22 °C)	k_{cat}/K_m(22 °C)	k_{cat}(5 °C)	k_{cat}/K_m(5 °C)
SLO	1.0 (0.1)	1.4 (0.1)	1.1 (0.3)	2.0 (0.2)
Q495E	0.99 (0.1)	1.1 (0.1)	n/d[b]	1.4 (0.1)
Q495A	0.90 (0.1)	1.1 (0.1)	0.84 (0.1)	1.4 (0.2)
Q697N	1.0 (0.1)	1.1 (0.1)	0.86 (0.1)	1.6 (0.1)
Q697E	0.70 (0.1)	0.74 (0.1)	0.73 (0.1)	1.1 (0.1)

[a] In 100 mM borate (pL 9.2). [b] Not determined (see the Results).

Solvent Isotope Effect. The kinetic parameters for all mutant enzymes were analyzed with LA-H31 in H_2O (pL 9.2) and D_2O (pL 9.2), at 5 and 22 °C, to determine if the mutant enzymes retained a solvent isotope-dependent step as part of the rate-determining step. The solvent isotope effect (SIE) for all four mutants was positive, though the magnitude of the effect for mutants was smaller than that for SLO, thus demonstrating a decrease in their hydrogen bond rearrangement dependency (Table 5). The SIE for SLO increased upon a decrease in temperature, which was consistent with previous results (*12*), showing that at lower temperatures, the solvent-dependent step for SLO becomes more rate-limiting. Q697N, Q495E, and Q495A exhibited increases in their k_{cat}/K_m SIE values with a decrease in temperature. Q697E exhibited an inverse k_{cat}/K_m of 0.74 ± 0.1 at 22 °C, which also increased with decreasing temperature by the same magnitude as those of the other enzymes. The k_{cat}/K_m measurements showed that a similar solvent-dependent step exists for all the mutant enzymes, and it becomes increasingly important as the temperature decreases.

Our k_{cat} SIE measurements of SLO showed that k_{cat} was fully limited by C−H bond cleavage of LA-H31 and independent of temperature, as also shown by Rickert et al. (*30*). Similar results were obtained for Q495E, Q495A, and Q697N, although error obscured possible deviations (Table 5). The k_{cat} SIE for Q697E, however, had a large inverse value (0.70 ± 0.1 at 22 °C), which was independent of temperature. To confirm these results, SIE experiments were also performed with LA-D31 to make C−H cleavage the sole rate-determining step (Table 6) (*12*). SLO exhibited no SIE for either k_{cat} or k_{cat}/K_m, indicating no solvent effect on C−H bond cleavage. Q697E, however, did show an inverse SIE, demonstrating that the C−H bond cleavage step in this control experiment is solely responsible for this effect.

EPR Spectra of Oxidized Mutant Lipoxygenases. The EPR spectra of all the SLO mutants, at 4.3 K, exhibited very weak $g \approx 4.3$ signals, which account for less than 1% of the total iron, because the mutants, as isolated, were in the reduced ferrous form, similar to the state of the native enzyme (*20*).

Table 6: Solvent Isotope Effect at 22 and 5 °C (H_2O/D_2O) with LA-D31[a]

	k_{cat}(22 °C)	k_{cat}/K_m(22 °C)	k_{cat}(5 °C)	k_{cat}/K_m(5 °C)
SLO	0.91 (0.1)	0.98 (0.1)	0.95 (0.1)	1.1 (0.1)
Q495E	0.97 (0.1)	0.85 (0.1)	n/d[b]	n/d[b]
Q495A	0.85 (0.1)	0.83 (0.1)	0.81 (0.1)	0.95 (0.1)
Q697N	0.96 (0.1)	0.87 (0.1)	0.89 (0.10)	1.1 (0.3)
Q697E	0.63 (0.1)	0.63 (0.1)	0.63 (0.1)	0.68 (0.1)

[a] In 100 mM borate (pL 9.2). [b] Not determined (see the Results).

Addition of approximately 1 equiv of 13-(*S*)-HPOD to the ferrous enzyme oxidized the iron to the catalytically competent ferric species. The second-coordination sphere mutants (Q495E, Q495A, Q697N, and Q697E) exhibited axial signals ($E/D = 0$), similar to that of SLO (*20*). These results were consistent with little or no perturbation of the iron environment by the second-coordination sphere mutations in the ferric oxidation state.

UV−Vis CD Spectroscopy. Oxidation of the mutant enzymes was accompanied by an increase in the visible absorbance intensity at approximately 400 nm [the yellow species, i.e., Fe(III) form]. This was assigned as a His−Fe(III) ligand-to-metal charge transfer (LMCT) transition as observed for other lipoxygenases (*20*). UV−vis CD spectroscopy resolved the LMCT band from the large protein envelope and revealed a well-isolated band, with a distinct maximum. The majority of the mutants (Q495E, Q495A, and Q697N) had maxima around 425 nm (23 800 cm^{-1}), similar to that of SLO (*20*). The LMCT of Q697E, however, was shifted to 416 nm (24 200 cm^{-1}), indicative of a decrease in the Lewis acidity and reduction potential of the iron. The change in Lewis acidity could not be associated with a change in the first coordination sphere of the metal, since the EPR spectra are unchanged. The introduction of a negative charge in the second coordination sphere is probably not responsible for the lower Lewis acidity of Q697E, as this was not observed for Q495E.

New Refinement of the Wild-Type Structure. A description of the original refinement of the SLO structure (PDB entry 1yge) was reported previously (*15*). This refinement was performed in X-PLOR 3.1 and utilized data for d_{min} values ranging between 10.0 and 1.4 Å with a $F/\sigma(F) \geq 2$ cutoff. It was anticipated that a subtle geometry difference, especially in Fe−ligand bond distances, might exist among the wild-type and mutant enzymes. Since it was unclear how different refinement protocols might affect subtle changes in the results, a uniform refinement protocol was adopted for all structures. Data with d_{min} values ranging from 20.0 Å to the high-resolution limit were used for each structural refinement, with no $F/\sigma(F)$ cutoff. A summary of active site bond lengths for the refined structures can be found in Table 7. An examination of these results reveals that the only significant change in Fe−ligand bond lengths for the wild-type structure is a contraction of the Fe−H_2O bond length, from 2.56 to 2.11 Å. This shorter distance is within the expected range of Fe(II)−ligand distances found in a survey of small molecule compounds (2.1−2.2 Å) (*16*). It is also similar (within the observed coordinate error) to the Fe(II)−O bond length of 2.04 Å found in a small molecule ferrous−methanol complex, which is an analogue of the iron site of lipoxygenases (*31*). The average of the Fe−H_2O bond lengths for all structures reported herein is 2.20 Å. This observed

Table 7: Selected Bond Distances (in angstroms)[a]

	wild type	Q495E	Q495A	Q697N	Q697E
Fe−N694	2.87	2.98	2.93	3.51	3.41
Fe−H690	2.29	2.11	2.17	2.20	2.24
Fe−H504	2.34	2.13	2.17	2.13	2.11
Fe−H499	2.21; 2.24	2.10	2.23	2.17	2.12; 2.41
Fe−I839	2.28	2.32	2.20	2.39	2.47
Fe−H_2O	2.11	2.29	2.10	2.25	2.26
N694−Q697	3.10	2.73	3.19	–	–
Q697−Q495	3.12	–	–	–	–
H499−E697	–	–	–	–	2.88
H499−E495	–	2.74	–	–	–

[a] Where more than one value is reported, the second value is for an alternate conformation of the H499 side chain.

contraction of the Fe−H_2O bond length in these structures is probably due to the difference in explicit nonbonding restraints used for waters in the two refinement programs. Seventeen alternate conformations were included in the wild-type model, including two conformations of approximately equivalent (0.56 vs 0.44) occupancy for the Fe ligand His_{499} (Figure 2a). These two conformations are related to each other by a rigid body movement of the imidazole ring about χ_1 of 11° and χ_2 of 35° relative to the Fe, and may reflect an inherent mobility of His_{499} for soybean lipoxygenase-1 Fe(II) sites. In this alternate conformation of His_{499}, a weak hydrogen bond (3.47 Å) is formed between histidine Nδ1 and Oϵ1 of Gln_{495}. Thus, the hydrogen-bonded network (Asn_{694}-Gln_{697}-Gln_{495}) appears to be extended to include His_{499} in the wild-type enzyme. The higher resolution of the wild-type structure may explain the observation of only the major conformation of His_{499} in the mutants (see below for an explanation of the alternate conformation observed in the Q697E mutant) (Table 1).

Gln_{697} Mutant Structures. The largest change in the ligand bond distances for the Fe(II) in the Gln_{697} mutants is the lengthening of the Fe−Asn_{694} distance by more than 0.5 Å from the wild-type structure (Figure 2b,c). This primarily occurs due to a rotation of the Asn_{694} carboxamide group relative to the Fe(II), and in the Q697N mutant, this may occur to facilitate a weak hydrogen bonding interaction with Asn_{697} Nδ2 (3.43 Å). The Asn_{697} side chain of the Q697N mutant adopts an unfavorable rotamer conformation to interact with Asn_{694}, and is too distant to interact with Gln_{495}. This Gln_{495} side chain does not participate in any bonding interactions with His_{499} or other parts of the protein, and appears to be quite flexible due to the weak electron density observed in the experimental maps. The side chain was modeled into the observed density, but displays relatively high isotropic thermal factors.

In the Q697E mutant, a significant deviation from octahedral symmetry about the iron is observed. The carboxylate group of Glu_{697} is rotated approximately 90° relative to the position of the glutamine carboxamide group in the wild-type enzyme. As a result, Glu_{697} Oϵ2 hydrogen bonds to an alternate conformation of the Fe−His_{499} ligand (Figure 2c); the relative occupancy of the two conformations is 0.56/0.44. Though this conformation also results from a rotation of the imidazole ring relative to the Fe(II), the rotation (139°) was about χ_2 only, and in the opposite direction from the one observed in the wild-type structure. As a result, Gln_{495} is not able to form a hydrogen bond with His_{499} in either conformation. The plane of His_{499} in the alternate conforma-

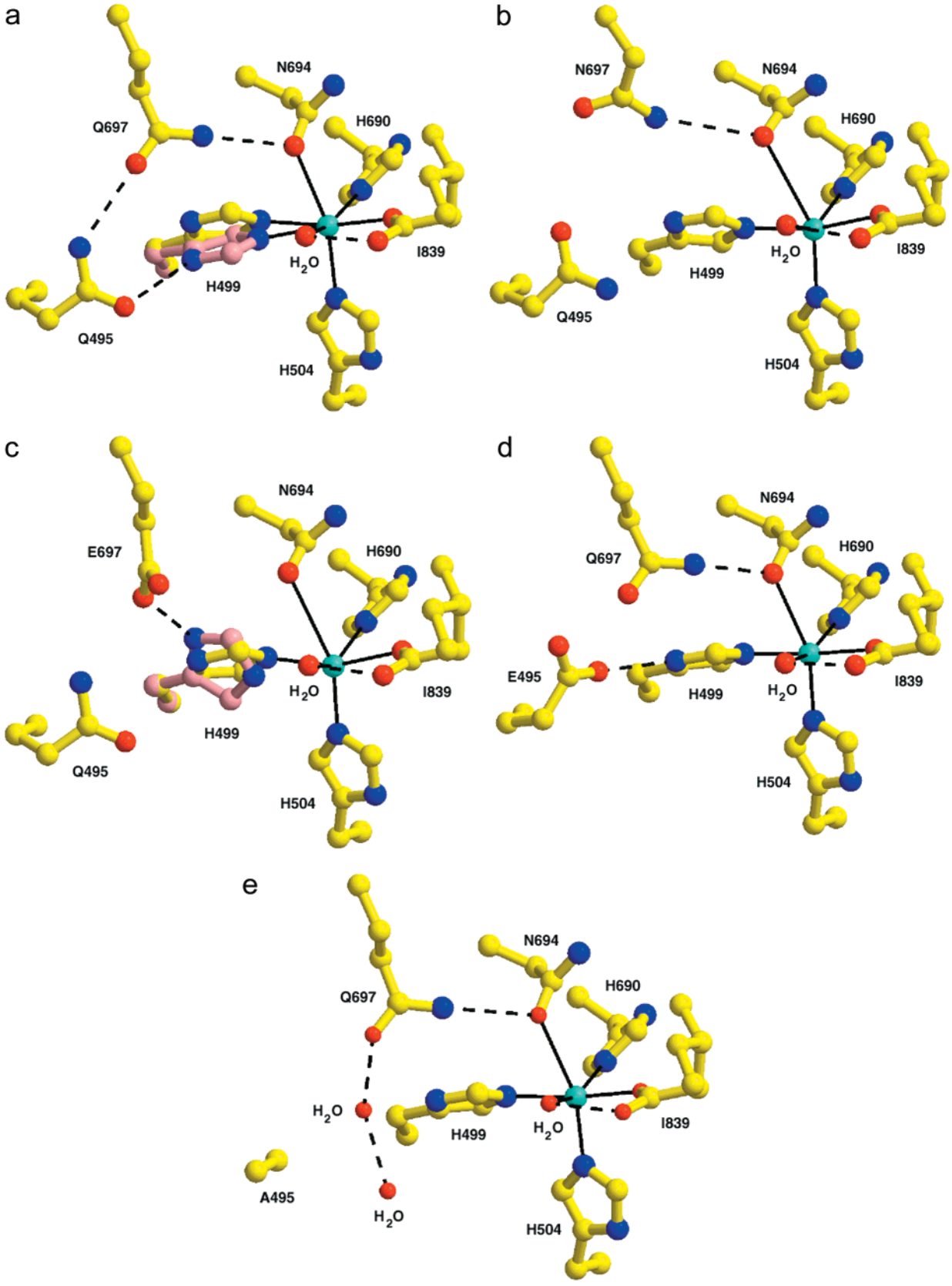

FIGURE 2: Coordination geometry of the Fe(II) centers of wild-type SLO (a), Q697N (b), Q697E (c), Q495E (d), and Q495A (e). Bonds between the iron and first-sphere ligands are drawn as solid lines, and hydrogen-bonding interactions are drawn as dashed lines. Oxygen atoms are drawn in red, nitrogens in blue, and carbons in yellow, and the iron atom is in cyan. The alternate conformations of His_{499} are shown in pink.

tion is oriented such that the His_{499} Nϵ2−Fe−Ile_{839} carboxylate oxygen angle is 148.6° (in the SLO structure, this angle is 167°) and the His_{499} Nϵ2−Fe−OH_2 angle is 70.4° (87° in the SLO). This significant deviation from octahedral symmetry may adversely affect the orbital overlap between His_{499} and the iron. The Fe(II)-bound OH_2 is also displaced in this

mutant toward Asn_{694} such that the His_{690} Nϵ2−Fe−OH_2 angle is 141° (157° in SLO).

Gln_{495} Mutant Structures. The coordination geometry of the Fe(II) (Table 7) in the two Gln_{495} mutants is virtually unchanged from that of the wild type. In the Q495A mutant, the Gln_{697}−Asn_{694} distance is similar to that of the wild-type, while in the Q495E mutant, this distance is contracted by 0.37 Å to 2.73 Å. Though spatially close, Oϵ1 of Glu_{495} is not in a favorable geometry to hydrogen bond to the side chain oxygen of Gln_{697}. Instead, Glu_{495} Oϵ2 hydrogen bonds to Nδ1 of the Fe ligand His_{499}, an interaction seen only for the alternate histidine conformation in the wild-type enzyme (Figure 2d). As a result, the negatively charged Glu_{495} side chain is in an orientation and position somewhat (though not exactly) similar to that of Gln_{495} in the wild-type enzyme. The resulting proximity of Glu_{495} may result in an electrostatic repulsion of Gln_{697}, which strengthens the Gln_{697}−Asn_{694} interaction, a phenomenon not observed in the Q495A structure.

Since the active site geometry of the Q495A structure is essentially unchanged from that of the wild type, the largest structural difference in this mutant is the absence of the Gln_{495} side chain, which has been replaced by four extra water molecules. One of these waters hydrogen bonds simultaneously to Gln_{697} and His_{499}, replacing the side chain in the hydrogen bond network (Figure 2e).

DISCUSSION

Klinman (*12*) and co-workers determined that at 15 °C the k_{cat}/K_m for SLO was rate-limited by three steps, substrate diffusion to the active site, hydrogen bond rearrangement (or water exclusion), and C−H bond cleavage; however, a detailed molecular mechanism of these steps remains elusive. To elucidate the mechanism of these steps, we chose to focus our investigation on the hydrogen bond network, which connects the substrate cavity to the iron coordination environment (Gln_{495} and Gln_{697}). This hydrogen bond network is present in both the SLO and 15-RLO structures and plays a steric role in positioning the inhibitor bound to 15-RLO. By analogy, this hydrogen bond network may also play a role in substrate positioning, and therefore, we generated mutants to test this hypothesis (Q495E, Q495A, Q697N, and Q697E).

The kinetic data of the four mutations indicate that changes in the hydrogen bond network may affect catalytic efficiencies, but the reaction mechanism remains the same. The results are in some cases subtle, but the trends are very clear. The k_{cat}/K_m KIE and viscosity dependence of Q495E show that its k_{cat}/K_m is dependent on multiple rate-limiting steps, similar to the case for SLO. The Q495A, Q697N, and Q697E mutants, however, have lower catalytic efficiencies. Their k_{cat}/K_m KIE values are relatively insensitive to temperature; their k_{cat}/K_m values are not sensitive to viscosity at 22 °C, while their absolute KIE values at 35 °C remain large, demonstrating a C−H bond cleavage mechanism similar to that of SLO. These data indicate that C−H bond cleavage (k_{cat}/K_m) is the sole rate-determining step at 22 °C for three mutants (Q495A, Q697N, and Q697E), but the molecular mechanism for cleavage remains unchanged.

The structural results, namely, a change at position Gln_{495}, suggest that the kinetic changes observed for these three mutants are due to an impairment of the precise substrate positioning required for optimum catalytic efficiency, which is consistent with observations for the L546A mutant (*30*). The structures of Q495A, Q697N, and Q697E reveal a common feature; the amino acid at position 495 is more flexible than in the SLO and Q495E structures, which results in a modification of the substrate docking site and probably the position of the bound substrate. Both Q697N and Q697E disrupt the hydrogen bond interactions among residue 697, Asn_{694}, and Gln_{495}, which results in a loss of structural stabilization to Gln_{495}. The loss of contact with Gln_{495} is significant because the interaction between Gln_{495} and His_{499} is weak, so Gln_{495} is isolated and therefore more flexible in both Q697N and Q697E than in SLO and Q495E. In the Q495A mutant, the side chain has been removed completely, thus enlarging the cavity considerably. The rate for these mutants is lowered because the substrate assumes unproductive conformations, but once the correct conformation is achieved, the C−H bond cleavage proceeds through the same tunneling mechanism as SLO (i.e., large KIE). Q495E has a stabilized side chain at position 495, similar to SLO, which provides a more rigid docking site for substrate binding and allows for the correct substrate conformation. This change in the hydrogen bond network is also a natural variant in 15-RLO (Glu_{357}), which supports our hypothesis that interaction of amino acid 495 with the hydrogen bond network is important to catalysis.

In light of these structural results, a model of linoleic acid was docked into the putative substrate cavity (Figure 3). The substrate was positioned with the hydrophobic end buried into the binding cavity, and the carboxylate end near the surface of the protein; the carbons that would be involved in the pentadienyl radical intermediate (C-9−C-13) were modeled as a planar unit. This places the *pro-S* hydrogen of C-11 of the substrate near the Fe(II)−OH_2 species ready for abstraction, with a 3.3 Å distance between the water position and C-11 (*30*). This distance is much longer than would be required for hydrogen abstraction by the Fe(III)−OH^- species and suggests a rearrangement of the substrate cavity environment upon oxidation and/or substrate binding. The site of oxygenation, C-13, is near Gln_{495}, Leu_{546}, and the alternate conformation of His_{499}. The C-14−C-18 hydrocarbon tail is flanked by the hydrophobic portion of the Gln_{495} side chain, while C-2−C-8 are positioned in a hydrophobic channel past Leu_{538}. The proper position of Gln_{495} and His_{499}, in addition to the hydrophobic residues that flank the pentadiene (Leu_{546}, Leu_{745}, Trp_{500}, and Leu_{538}), may provide a very specific binding pocket for the substrate, which would facilitate catalysis. Disrupting this binding pocket by changing the position of Gln_{495} may affect the proper positioning of the substrate for C−H bond cleavage so that abstraction becomes more rate-limiting, as is observed in the Q495A, Q697N, and Q697E mutants, and in the previously mentioned L546A mutant (*17*).

The hydrogen bond network among residues 694, 697, and 495 also plays a role in the hydrogen bond rearrangement of the enzymatic mechanism. The hydrogen bond network for all four mutants has been disrupted, and the absolute SIE values have been decreased, relative to that of SLO, indicating a possible rearrangement upon substrate interaction with Gln_{495}. This result does not explain the fact that all four mutants still exhibit increased SIE values with temperature

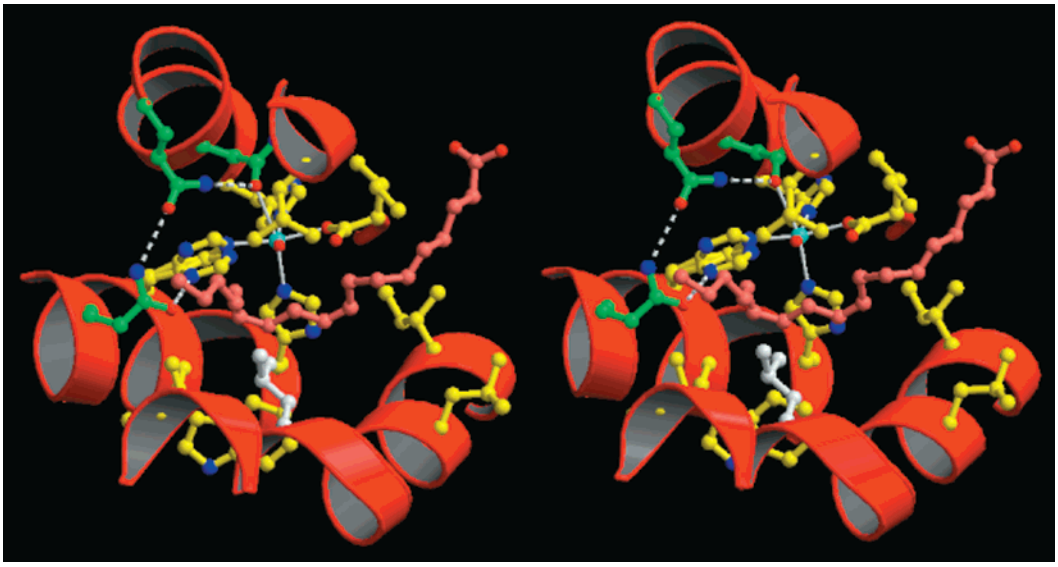

FIGURE 3: Stereoview of a model of linoleic acid in the putative active site of wild-type SLO. The iron atom is colored cyan and the linoleic acid pink; the residues that form the hydrogen bonding network (Asn_{694}, Gln_{697}, and Gln_{495}) are green, and Leu_{546} is white. Bonds between the iron and first-sphere ligands are drawn as solid lines, and hydrogen-bonding interactions are drawn as dashed lines.

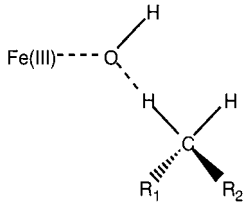

FIGURE 4: Model of the newly proposed C−H bond cleavage transition state for Fe(III)−OH^-.

decreases, and may indicate water exclusion from the active site as an additional factor in the mechanism. This hypothesis needs to be investigated further by proton inventory experiments, which may help define the number and nature of the protons involved in the SIE for SLO and the four mutants.

The inverse SIE observed for Q697E is significant and is solely dependent on the hydrogen atom abstraction. Similar inverse solvent isotope effects have been previously observed for Zn-metalloproteins and have been shown to be due to a metal−hydroxide active site base through determination of their fractionation factors (*32*). This hypothesis could account for the observed inverse SIE of Q697E, since an Fe(III)−OH^- active site base has already been proposed on the basis of spectroscopic measurements but has never been observed kinetically (*16*). The fact that an inverse SIE is not observed for SLO shows a difference in the fractionation factors between SLO and Q697E. This difference is possibly due to a change in the Lewis acidity of the iron site because the Lewis acidity of the Fe(III)−OH^- and Fe(II)−OH_2 species will affect their fractionation factors and subsequently their overall SIE values (*32*). The LMCT band for Q697E is blue shifted to 416 nm from the value of 425 nm of SLO, which indicates a lower Lewis acidity of the ferric iron (*20*). The lower Lewis acidity of Q697E causes an increase in the Fe(II)−OH_2 pK_a and hence a decrease in the value of the SIE. This result is the first kinetic evidence for an Fe(III)−OH^- active site base in the lipoxygenase mechanism and allows us to propose a new transition state model (Figure 4). This transition state requires substrate positioning close enough to the Fe(III)−OH^- species to allow for tunneling of the hydrogen atom to the metal-bound hydroxide and would account for all the data currently in the lipoxygenase literature. This hypothesis needs to be further tested experimentally by direct measurements of the fractionation factors for both SLO and Q697E via NMR, as was previously done with the cobalt-substituted carbonic anhydrase (*33*).

In conclusion, a combination of kinetic and structural investigations of various SLO mutants have allowed us to kinetically isolate the C−H bond cleavage step and provide a refined explanation of the SLO mechanism of action. Efficient C−H bond cleavage is achieved by the correct positioning of the substrate through steric interactions with the side chain of Gln_{495}, and the hydrogen bond network of Gln_{495}, Gln_{697}, and Asn_{694} is responsible for the hydrogen bond rearrangement step after substrate binding. The inverse SIE for Q697E represents the first kinetic evidence that the Fe(III)−OH^- species is the active site base for hydrogen atom abstraction and allows us to propose a new transition state model which involves direct interaction between the iron site and the substrate. These discoveries represent an advance in the understanding of the molecular mechanism of lipoxygenase and help establish the molecular framework for further investigations.

ACKNOWLEDGMENT

Thanks are given to M. Knapp and J. Klinman for helpful discussions and to J. Williams for technical support. We also thank Andrzej Joachimiak and the staff of the Structural Biology Center beamline (19-ID) at the Advanced Photon Source for assistance in X-ray data collection. Use of the Argonne National Laboratory Structural Biology Center beamlines at the Advanced Photon Source was supported by the U.S. Department of Energy, Office of Biological and Environmental Research, under Contract W-31-109-ENG-38.

REFERENCES

1. Gardner, H. W. (1991) *Biochim. Biophys. Acta 1084*, 221−239.

2. Siedow, J. N. (1991) *Annu. Rev. Plant Physiol. Plant Mol. Biol. 42*, 145−188.
3. Samuelsson, B., Dahlen, S. E., Lindgren, J. A., Rouzer, C. A., and Serhan, C. N. (1987) *Science 237*, 1171−1176.
4. Sigal, E. (1991) *J. Am. Phys. Soc. 260*, 13−28.
5. Harats, D., Shaish, A., George, J., Mulkins, M., Kurihara, H., Levkovitz, H., and Sigal, E. (2000) *Arterioscler., Thromb., Vasc. Biol. 20*, 2100−2105.
6. Steele, V. E., Holmes, C. A., Hawk, E. T., Kopelovich, L., Lubet, R. A., Crowell, J. A., Sigman, C. C., and Kelloff, G. J. (1999) *Cancer Epidemiol., Biomarkers Prev. 8*, 467−483.
7. Gosh, J., and Myers, C. E. (1998) *Proc. Natl. Acad. Sci. U.S.A. 95*, 13182−13187.
8. Nie, D., Hillman, G. G., Geddes, T., Tang, K., Pierson, C., Grignon, D. J., and Honn, K. V. (1998) *Cancer Res. 58*, 4047−4051.
9. DeGroot, J. J. M. C., Aasa, R., Malmstrom, B. G., Slappendel, S., Veldink, G. A., and Vliegenthart, J. F. G. (1975) *Biochim. Biophys. Acta 377*, 71−79.
10. Solomon, E. I., Zhou, J., Neese, F., and Pavel, E. G. (1997) *Chem. Biol. 4*, 795−808.
11. Gardner, H. W. (1989) *Biochim. Biophys. Acta 1001*, 274−281.
12. Glickman, M. H., and Klinman, J. P. (1995) *Biochemistry 34*, 14077−14092.
13. Boyington, J. C., Gaffney, B. J., and Amzel, L. M. (1993) *Science 260*, 1482−1486.
14. Minor, W., Steczko, J., Bolin, J. T., Otwinowski, Z., and Axelrod, B. (1993) *Biochemistry 32*, 6320−6323.
15. Minor, W., Steczko, J., Boguslaw, S., Otwinowski, Z., Bolin, J. T., Walter, R., and Axelrod, B. (1996) *Biochemistry 35*, 10687−10701.
16. Scarrow, R. C., Trimitsis, M. G., Buck, C. P., Grove, G. N., Cowling, R. A., and Nelson, M. J. (1994) *Biochemistry 33*, 15023−15035.
17. Gillmor, S. A., Villasenor, A., Fletterick, R., Sigal, E., and Browner, M. (1997) *Nat. Struct. Biol. 4*, 1003−1009.
18. Pham, C., Jankun, J., Skrzypczak-Jankun, E., Flowers, R. A., and Funk, M. O. (1998) *Biochemistry 37*, 17952−17957.
19. Pavlosky, M. A., Zhang, Y., Westre, T. E., Gan, Q.-F., Pavel, E. G., Campochiaro, C., Hedman, B., Hodgson, K. O., and Solomon, E. I. (1995) *J. Am. Chem. Soc. 117*, 4316−4327.
20. Holman, T. R., Zhou, J., and Solomon, E. I. (1998) *J. Am. Chem. Soc. 120*, 12564−12572.
21. Mogul, R., Johansen, E., and Holman, T. (2000) *Biochemistry 39*, 4801−4807.
22. Lewis, E. R., Johansen, E., and Holman, T. R. (1999) *J. Am. Chem. Soc. 121*, 1395−1396.
23. Steczko, J., Muchmore, C. R., Smith, J. L., and Axelrod, B. (1990) *J. Biol. Chem. 265*, 11352−11354.
24. Naday, I., Ross, S., Westbrook, E. M., and Zentai, G. (1998) *Opt. Eng. 37*, 1235−1244.
25. Otwinowski, Z., and Minor, W. (1997) *Methods Enzymol. 276*, 307−326.
26. French, S., and Wilson, K. (1978) *Acta Crystallogr. A34*, 517−525.
27. Project, C. C. (1994) *Acta Crystallogr. D50*, 760−763.
28. Brünger, A. T., Adams, P. D., Clore, G. M., DeLano, W. L., Gros, P., Grosse-Kunstleve, R. W., Jiang, J.-S., Kuszewski, J., Nilges, M., Pannu, N. S., Read, R. J., Rice, L. M., Simonson, T., and Warren, G. L. (1998) *Acta Crystallogr. D54*, 905−921.
29. Jones, T. A., Zou, J. Y., Cowan, S. W., and Kjeldgaard, M. (1991) *Acta Crystallogr. A47*, 110−119.
30. Rickert, K. W., and Klinman, J. P. (1999) *Biochemistry 38*, 12218−12228.
31. Jonas, R. T., and Stack, T. D. P. (1997) *J. Am. Chem. Soc. 119*, 8566−8567.
32. Quinn, D. M., and Sutton, L. D. (1991) in *Enzyme Mechanism from Isotope Effects* (Cook, P. F., Ed.) pp 73−126, CRC Press, Boca Raton, FL.
33. Kassebaum, J. W., and Silverman, D. N. (1989) *J. Am. Chem. Soc. 111*, 2691−2696.

BI002893D